

# Fermi arc criterion for surface Majorana modes in superconducting time-reversal symmetric Weyl semimetals

Rauf Giwa, Pavan Hosur<sup>1</sup>

<sup>1</sup>*Department of Physics, University of Houston, Houston 77204, USA*

Many clever routes to Majorana fermions have been discovered by exploiting the interplay between superconductivity and band topology in metals and insulators. However, realizations in semimetals remain less explored. We ask, “under what conditions do superconductor vortices in time-reversal symmetric Weyl semimetals – three-dimensional semimetals with only time-reversal symmetry – trap Majorana fermions on the surface?” If each constant- $k_z$  plane, where  $z$  is the vortex axis, contains equal numbers of Weyl nodes of each chirality, we predict a generically gapped vortex and derive a topological invariant  $\nu = \pm 1$  in terms of the Fermi arc structure that signals the presence or absence of surface Majorana fermions. In contrast, if certain constant- $k_z$  planes contain a net chirality of Weyl nodes, the vortex is gapless. We analytically calculate  $\nu$  within a perturbative scheme and provide numerical support with a lattice model. The criteria survive the presence of other bulk and surface bands and yield phase transitions between trivial, gapless and topological vortices upon tilting the vortex. We propose  $\text{Li}(\text{Fe}_{0.91}\text{Co}_{0.09})\text{As}$  and  $\text{Fe}_{1+y}\text{Se}_{0.45}\text{Te}_{0.55}$  with broken inversion symmetry as candidates for realizing our proposals.

The interplay of band topology and superconductivity has paved new routes to Majorana fermions (MFs) – as topologically protected zero energy bound states trapped in topological defects such as superconductor vortices [1–5, 8–16, 18–20]. Following realizations in semiconductor nanowire-superconductor heterostructures [11, 14, 21], MFs were recently found for the first time in a three-dimensional (3D) system – at the ends of vortices in the bulk superconductor  $\text{FeSe}_{0.45}\text{Te}_{0.55}$  [22–26]. This inspires a fundamental question: in a 3D superconductor, what properties of the normal state band structure ensure that vortices trap protected MFs at their ends? Restricting to bands with time-reversal symmetry ( $\mathcal{T}$ ), since  $\mathcal{T}$  enables a Cooper instability to begin with, sufficient conditions are known in two generic cases: a band insulator (metal) yields MFs if it is topological [2] (a modestly doped topological insulator [3]).

The third type of generic  $\mathcal{T}$ -preserving band material is a time-reversal symmetric Weyl semimetal (TWSM) [27–30]. Here, point intersections between non-degenerate bands create Weyl nodes (WNs) that possess a chirality of  $\pm 1$  and appear in quadruplets to respect  $\mathcal{T}$  and Brillouin zone periodicity. Weyl semimetals constitute topological matter as they are immune to perturbations that do not hybridize anti-chiral WN, i.e., WN of opposite chirality and exhibit numerous topological responses [31–57]. On the surface, the bulk band topology manifests as Fermi arcs (FAs) that connect surface projections of anti-chiral WN.

Motivated by the quest for MFs, we ask, “what is the fate of a superconductor vortex in a TWSM?” We show that there are three possible vortex phases – (i) gapped, with end-MFs; (ii) gapped, without end-MFs; (iii) gapless, with topologically protected chiral MFs dispersing along the vortex axis  $\hat{z}$ . Crucially, we prove that the vortex phase relies solely on basic band structure data, namely, the FA configuration on the surface normal to  $\hat{z}$  and the locations of the bulk WN. Remarkably, simply tilting the vortex can

drive transitions between the three phases.

The criteria for the phases are as follows (see Fig. 1). Within each constant- $k_z$  plane, identify the pair(s) of anti-chiral WN that are closest to each other in periodic  $\mathbf{k}$ -space. Connect the partners with a geodesic and project it onto the surface. From the remaining WN, identify the next closest pair(s) and project their geodesic(s) onto the surface, and so on for all WN and constant- $k_z$  planes. If all the WN find partners in this process, the surface Brillouin zone will contain a set of lines that, along with the FAs, form closed *Fermi-geodesic loops*. In general, the surface will also carry closed Fermi loops and Dirac nodes. If the total number of Fermi-geodesic loops, Fermi loops and Dirac nodes is  $M$ , we predict a gapped vortex with a topological invariant

$$\nu = (-1)^M \quad (1)$$

Thus, odd  $M$  yields a topologically protected MF in the vortex core on the surface whereas even  $M$  does not. All WN find partners only if each constant- $k_z$  plane contains equal numbers of left- and right-handed WN. For a minimal TWSM with four WN at  $(\pm \mathbf{K}_1, \pm \mathbf{K}_2)$ , a vortex direction such that  $|K_{1z}| = |K_{2z}|$  ensures this, while general TWSMs with more WN need a mirror or glide symmetry plane parallel to  $\hat{z}$  – which is present in most TWSMs [45, 58–60] – to ensure all WN are partnered. Generically, though, some WN will lack partners and the surface will host open *Fermi-geodesic arcs* whose end-points will be projections of the unpartnered WN. Each such WN will contribute a 1D chiral MF to the bulk vortex spectrum with a chirality equal to its own chirality times the vorticity of  $\pm 1$ . The vortex will be in a gapless phase protected by  $k_z$ -conservation, analogous to the topological protection of a Weyl semimetal by 3D momentum conservation.

These criteria hold for general pairing symmetries provided the superconductor is gapped in the absence of a vortex. They survive doping around the WN if the resulting

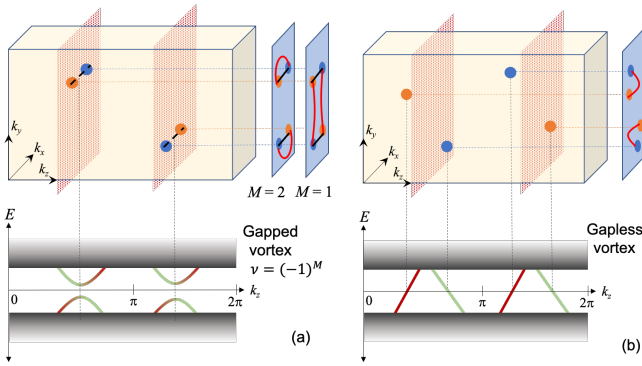


Figure 1. Schematic of the main result. Orange (blue) dots denote right(left)-handed WNs which produce right(left)-moving chiral MFs, colored red (green), inside the vortex. To determine the vortex phase, identify pairs of anti-chiral WNs at the same  $k_z$  and project the line joining them onto the surface. If these lines (solid black), along with the FAs (red curves), form  $M$  closed loops, the vortex is gapped and has a topological invariant  $\nu = (-1)^M$  (a), whereas open arcs produce a gapless vortex (b).

Fermi surfaces are well-separated and the presence of trivial Fermi surfaces with rare exceptions. They are also immune to surface effects unless the surface is exposed to a topological insulator, in which case  $M$  effectively acquires the odd number of surface Fermi loops or Dirac nodes of the latter. Finally, (1) captures the known results for metals [3] and insulators [2], which lack Fermi-geodesic contours but may have Fermi loops and Dirac nodes.

Eq. (1) is obtained by computing the  $\mathbb{Z}_2$  topological invariant for the vortex viewed as a 1D superconductor [5, 61, 62]. We require a mild assumption in the clean limit: for a given WN, if the two nearest anti-chiral WNs at the same  $k_z$  are at distances  $\Delta K_1$  and  $\Delta K_2$ , then  $e^{\frac{\hbar\xi}{\Delta_0}[v_1(\Delta K_1)^2 - v_2(\Delta K_2)^2]} \gg 1$  or  $\Delta K_1 \gtrsim \Delta K_2$ , where  $\Delta_0$  and  $\xi$  are superconducting properties – the uniform pairing amplitude and coherence length, respectively – and  $v_i$  is the typical Weyl velocity along  $\Delta K_i$ . This condition ensures that the dominant hybridization is between chiral MFs from neighboring anti-chiral WNs, assuming hybridization is driven by band curvature. If hybridization is due to non-magnetic disorder that is smooth over distance  $\ell_D$ , the requirement becomes  $\Delta K_1 \gg \ell_D^{-1} \gg \Delta K_2$  while magnetic disorder invalidates (1). Disorder can be suppressed in principle whereas band curvature is unavoidable, so a physical regime of validity of (1) exists. We neglect hybridization between equi-chiral chiral MFs, i.e., chiral MFs of the same chirality, which amounts to smoothly deforming any accidentally gapless non-chiral vortex mini-bands away from zero energy.

Heuristically, (1) says that vortex-end MFs are present (absent) if the TWSM normal state is “closer” to a topological (trivial) insulator. To see this, imagine moving the WNs along the geodesics and annihilating them in pairs. If all WNs get annihilated, the resulting insulator will be

topological (trivial) if the surface FAs evolve into an odd (even) number of surface Fermi loops, while the vortex will be topological (trivial). However, the vortex spectrum remains gapped in the process, so its topological state before and after WN-annihilation must be the same.

Recently, Refs. [63, 64] showed that  $s$ -wave superconductor vortices in Dirac semimetals can trap helical MFs protected by crystal symmetries. Unlike those vortices, the gapless vortex here is a 1D phase of matter rather than a critical point as it cannot be gapped out by perturbatively changing the crystal space group. Ref. [65] found that below a critical doping in a lattice model of a Dirac semimetal with two Dirac nodes, an  $s$ -wave vortex normal to the line joining the nodes is gapped and traps a surface MF. The MF survives when the Dirac semimetal is perturbed into a minimal TWSM with four WNs in the plane normal to the vortex, assuming  $s$ -wave pairing even with broken inversion symmetry ( $\mathcal{I}$ ) in the TWSM. In comparison, our criteria include the TWSM results of Ref. [65] at low doping, but allow arbitrary numbers and configurations of type-I WNs, trivial Fermi surfaces and filled topological bands in the bulk, FAs, Fermi loops and Dirac nodes on the surface, and arbitrary pairing that opens a full gap when uniform.

*Continuum analytics:*– Consider a canonical WN of chirality  $h = \pm 1$  described by  $H_W(\mathbf{P}) = h \sum_j v_j \Sigma_j P_j - \mu$ , where  $\Sigma_j$ ,  $j = X, Y, Z$ , are Pauli matrices spanning the lowest two bands and  $\mathbf{P}$  is the momentum relative to the WN. At  $P_Z = 0$ ,  $H_W$  resembles the 2D surface Hamiltonian of a 3D topological insulator [2, 3, 66]. If  $v_X = v_Y$  and  $\mu = 0$ , it yields a pseudospin-polarized MF with  $\langle \Sigma_Z \rangle = w$  in the core of an  $s$ -wave superconductor vortex,  $\Delta(\mathbf{R}) = \Delta(R)e^{iw\Theta}$ ,  $w = \pm 1$  [2]. Being topologically protected, the MF will survive albeit with partial polarization,  $0 < w \langle \Sigma_Z \rangle < 1$ , when  $v_X \neq v_Y$ ,  $\mu \neq 0$  and the pairing is arbitrary but real and non-zero on the Fermi surface. In fact, the MF only requires a Fermi surface Berry phase of  $\pi$  in the weak-pairing, smooth-vortex limit [3]. When  $P_Z \neq 0$ , the MF disperses as  $E_h = \hbar v_Z P_Z \langle \Sigma_Z \rangle$ , thus realizing a chiral MF with chirality  $h$  at  $P_Z = 0$  or the  $k_z$  of the parent WN. In a real TWSM,  $k_z$ -conservation forbids hybridization between chiral MFs whose parent WNs are at different  $k_z$ , resulting in a gapless vortex [Fig. 1(b)].

Next, consider a minimal TWSM with one quadruplet of WNs at  $(\pm \mathbf{K}_1, 0)$ ,  $(\pm \mathbf{K}_2, 0)$ , where WNs at  $\pm \mathbf{K}_n$  are related by  $\mathcal{T}$  and have chirality  $(-1)^n$ . Suppose FAs on the  $z = 0$  surface connect  $\mathbf{K}_1$  to  $\mathbf{K}_2$  and  $-\mathbf{K}_1$  to  $-\mathbf{K}_2$ , and Fermi surfaces around the WNs are well-separated. In the presence of a superconductor vortex along  $\hat{\mathbf{z}}$ , each WN produces a chiral MF dispersing along  $(-1)^n \hat{\mathbf{z}}$  with a wavefunction  $\psi_{\pm n} = e^{i\mathbf{K}_n \cdot \mathbf{r}} \varphi_n(\mathbf{r})$ , where  $\varphi_n(\mathbf{r})$  is the zero mode of the vortex Hamiltonian near the  $n^{\text{th}}$  WN. The chiral MFs remain robust when  $|\mathbf{K}_n \xi| \rightarrow \infty$ , but hybridize for finite  $|\mathbf{K}_n \xi|$ . Neglecting hybridization between equi-chiral chiral MFs, a generic perturbation  $H'$  in the basis  $(\psi_{+1}, \psi_{-1}, \psi_{+2}, \psi_{-2})^T$  has the form  $H' =$

$\begin{pmatrix} 0 & iQ \\ -iQ^\dagger & 0 \end{pmatrix}$  where  $Q = \begin{pmatrix} q_{12} & q_{1\bar{2}} \\ q_{\bar{1}2} & q_{\bar{1}\bar{2}} \end{pmatrix}$  and  $q_{mn} = \langle \psi_m | H' | \psi_n \rangle$ . If  $H'$  preserves  $\mathcal{T}$ , then  $q_{mn} = q_{\bar{m}\bar{n}}$  and the vortex is a gapped 1D superconductor with topological invariant  $\nu = \text{sgn}(\text{Pf}[H']) = \text{sgn}(|q_{12}|^2 - |q_{1\bar{2}}|^2)$  [5]. For a spatially smooth perturbation,  $q_{mn}$  decays with  $|\mathbf{K}_m - \mathbf{K}_n|$ ; for instance, band curvature terms yield  $q_{mn} \sim e^{-\frac{1}{2}|\mathbf{K}_m - \mathbf{K}_n|^2 \xi / \Delta_0}$  for a linear vortex profile with slope  $\Delta_0 / \xi$  [67]. Then,  $|\mathbf{K}_1 - \mathbf{K}_2| \lesssim |\mathbf{K}_1 + \mathbf{K}_2|$  produces a trivial vortex while  $|\mathbf{K}_1 - \mathbf{K}_2| \gtrsim |\mathbf{K}_1 + \mathbf{K}_2|$  yields a topological vortex with end MFs. On the surface, geodesics connecting  $\mathbf{K}_1$  to  $\mathbf{K}_2$  and  $-\mathbf{K}_1$  to  $-\mathbf{K}_2$ , along with the FAs, form  $M = 2$  loops. In contrast, geodesics connecting  $\mathbf{K}_1$  to  $-\mathbf{K}_2$  and  $-\mathbf{K}_1$  to  $\mathbf{K}_2$  form  $M = 1$  loops with the FAs. Thus, there is a one-to-one correspondence between  $\nu$  and  $M$  that is captured by (1). The Gaussian form of  $q_{mn}$  further ensures only logarithmic corrections to the above inequalities due to  $\mathcal{O}(1)$  pre-factors.

Next, consider moving the WNs away from  $k_z = 0$  in pairs while preserving  $\mathcal{T}$  in the normal state. If  $K_{1z} = K_{2z}$ , the chiral MF  $\psi_{+1}(\mathbf{r})$  can hybridize with  $\psi_{+2}(\mathbf{r})$  but not with  $\psi_{-2}(\mathbf{r})$ , so the resulting vortex is adiabatically connected to the trivial vortex where all WNs are at  $k_z = 0$ ,  $q_{12} \neq 0$  and  $q_{1\bar{2}} = 0$ . In contrast, if  $K_{1z} = -K_{2z}$ , the adiabatic equivalent with all WNs at  $k_z = 0$  has  $q_{1\bar{2}} \neq 0$  and  $q_{12} = 0$ , which is a topological vortex. These conclusions extend straightforwardly to more quadruplets of WNs, thus proving (1) for arbitrary configurations of WNs and FAs.

Finally, let us consider the effects of additional bands on our criteria. A filled topological band will produce a 2D Dirac node or Fermi loop on the surface in the normal state, thereby changing the parity of  $M$ . However, the superconductor vortex will trap another surface MF and acquire a bulk gap due to this band, thus preserving (1). Suppose the bulk also contains trivial Fermi surfaces, i.e., Fermi surface that do not enclose WNs or other band intersections. For pairing that is real and non-zero on the Fermi surface, a vortex will contain bands  $\varepsilon_n(k_z) \sim \frac{\Delta_0}{\xi l_F(k_z)} \left( n + \frac{1}{2} + \frac{\phi_F(k_z)}{2\pi} \right)$  for each trivial Fermi surface, where  $n \in \mathbb{Z}$  and  $l_F(k_z)$  ( $\phi_F(k_z)$ ) is the perimeter (Berry phase) of the Fermi surface cross-section at  $k_z$  [3]. Unless  $\phi_F(k_z) = 0$ , trivial Fermi surfaces come in pairs with opposite Berry phases  $\pm \phi_F(k_z)$  to ensure that the constant- $k_z$  slice is a sensible 2D metal. As a result, slices with  $\phi_F(k_z) \neq \pi$  will acquire a vortex minigap  $\sim \Delta_0 / \xi l_F(k_z)$  while slices with  $\phi_F(k_z) = \pm \pi$ , where the minigap vanishes, will host counter-propagating chiral MFs that will generically hybridize and gap out. In summary, additional bands will not interconvert gapped and gapless vortices and filled bands always preserve our general criteria.

For gapped vortices, predicted to obey (1), curable violations due to trivial Fermi surfaces occur in two cases: (i) a surface Fermi loop or Dirac node gets buried under the surface projection of a bulk Fermi surface, resulting in  $M_{\text{observable}} = M - 1$ . This can be cured in principle by dop-

ing to expose the relevant surface state; (ii) a Fermi surface centered at  $k_z = 0$  or  $\pi$  is past the doping threshold for a vortex phase transition [3], which changes the vortex phase without changing  $M$ . This can be fixed by noting that such a Fermi surface has a pair of slices away from  $k_z = 0, \pi$  where  $\phi_F(k_z) = \pi$ . An incurable violation occurs when  $\phi_F(k_z) = \pi$  at the precise  $k_z$  where a WN exists, the WN is closer to the trivial Fermi surface than to other anti-chiral WNs at the same  $k_z$  and the chiral MFs produced by the trivial Fermi surface and the WN have opposite chiralities. Then,  $H'$  must include hybridization between these MFs, but (1) is ruined because  $M$  stays unchanged.

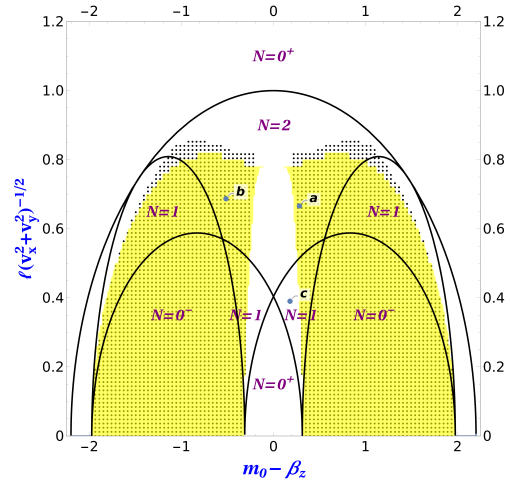


Figure 2. Vortex topological phases predicted by (1) and computed numerically. The yellow mask (black dots) denote a vortex predicted (computed) to be topological. Black lines separate the normal states: TWSMs with  $N = 1, 2$  quadruplets of WNs at  $k_z = 0$  and trivial/topological ( $N = 0^\pm$ ) insulators. We fix  $v_{x,y} = 1.18, .856$ ,  $\beta_{x,y,z} = .856, 1.178, 3.0$ ,  $\Delta(r) = 0.42 \tanh(0.3r)$  and  $L_{x,y} = 31$ . Points **t**, **m** and **b** are further studied in Fig. 3

*Lattice numerics:-* We support our general claims with numerics on an orthorhombic lattice model defined by  $H(\mathbf{k}) = \tau_x \boldsymbol{\sigma} \cdot \mathbf{d}(\mathbf{k}) + \tau_z m(\mathbf{k}) - \tau_y \sigma_z \ell$  where  $d_i = v_i \sin k_i$ ,  $i = x, y, z$ ,  $m(\mathbf{k}) = m_0 - \sum_i \beta_i \cos k_i$  and  $\tau_i$  ( $\sigma_i$ ) are Pauli matrices in orbital (spin) space. Varying  $\beta_{x,y,z}$  and  $\ell$  allows tuning into trivial and topological insulating phases as well as TWSMs with up to two quadruplets of WNs each at  $k_z = 0, \pi$  at the Fermi level. We then introduce an  $s$ -wave superconductor vortex  $\Delta(\mathbf{r}) = |\Delta(r)| e^{i\theta}$  and diagonalize the Bogoliubov-deGennes Hamiltonian in 2D real space at fixed  $k_z$  to obtain the spectrum and the topological invariant [5] for a class D 1D superconductor [61, 62]. In [67], we describe graphical methods for determining the normal state of  $H(\mathbf{k})$  and FA-configuration as well as further details of the lattice numerics. Fig. 2 shows that the prediction using (1) agrees excellently with the explicit calculation. We found smaller mismatch for larger systems or weaker pairing, suggesting that it is due to departure from the thermodynamic and weak-pairing limits.



Fig. 3 shows the Fermi-geodesic loops in the normal state and the probability density of the lowest few vortex modes for select points in Fig. 2. The FAs are obtained by plotting the lowest energy at each surface momentum in the normal phase and the geodesics are simply straight lines connecting proximate anti-chiral WNs at  $k_z = 0$ . The probability densities are computed by diagonalizing the vortex Hamiltonian in 3D real space. For each selected point, we find that the number of MFs localized to the vortex ends equals  $M$ . In Fig. 4, we show that tilting the vortex drives phase transitions between trivial, topological and gapless vortices since geodesics connect WNs at the same  $k_z$ . The transitions are expected at infinitesimal tilting in the weak-pairing, smooth-vortex limit, while the numerics find the transitions to occur at small angles.

**Candidate material:-** We propose  $\text{Li}(\text{Fe}_{0.91}\text{Co}_{0.09})\text{As}$  and  $\text{Fe}_{1-y}\text{Se}_{0.45}\text{Te}_{0.55}$  with broken  $\mathcal{I}$  as candidate materials.  $\text{Li}(\text{Fe}_{0.91}\text{Co}_{0.09})\text{As}$  is a Dirac semimetal with two Dirac nodes on the  $c$ -axis of the crystal [68] and shows strongly type-II superconductivity below  $T_c \approx 9K$  [69].  $\text{FeSe}_{0.45}\text{Te}_{0.55}$  realizes a doped topological insulator that turns into a type-II superconductor below  $T_c \approx 14.5K$  [25, 26], but the normal state also has two Dirac nodes along the  $c$ -axis  $\sim 15meV$  above the Fermi level that may be accessed with naturally occurring Fe-dopants [68]. Perturbatively breaking  $\mathcal{I}$  while preserving  $\mathcal{T}$  will turn the Dirac semimetals into a TWSM with four WNs at  $\pm\mathbf{K}_1, \pm\mathbf{K}_2$  with  $K_1^c \approx K_2^c \gg |\mathbf{K}_1 - \mathbf{K}_2|$ . If superconductivity survives  $\mathcal{I}$ -breaking, a vortex along  $\hat{z}$  will be topological (trivial) according to (1) if  $|K_{1z}| = |K_{2z}|$  and  $(\hat{z} \times \mathbf{K}_1) \cdot (\hat{z} \times \mathbf{K}_2) > 0 (< 0)$ , whereas a vortex in any other direction will be gapless. Assuming typical values  $v \sim 10^5 m/s$  for the Dirac velocity, chemical potential  $\mu \sim 100K$  relative to the WNs,  $\Delta_0 \sim 5K$ ,  $\xi \sim 5nm \ll$  the penetration depth  $d \sim 10^2 nm$  observed in  $\text{LiFeAs}$  [64] which guarantees negligible inter-vortex tunneling ( $\propto e^{-d/\xi}$ ), and  $|\mathbf{K}_1 - \mathbf{K}_2|/K_1^c \approx 0.1$ , we estimate a vortex gap of  $\sim 0.1K$ . However, the gap depends exponentially on  $\xi$ ,  $|\mathbf{K}_1 - \mathbf{K}_2|$  and  $\Delta_0$ , so it will change substantially for small changes in their values [67].

We acknowledge financial support from the Department of Physics and the College of Natural Sciences and Mathematics, University of Houston and NSF-DMR-2047193.

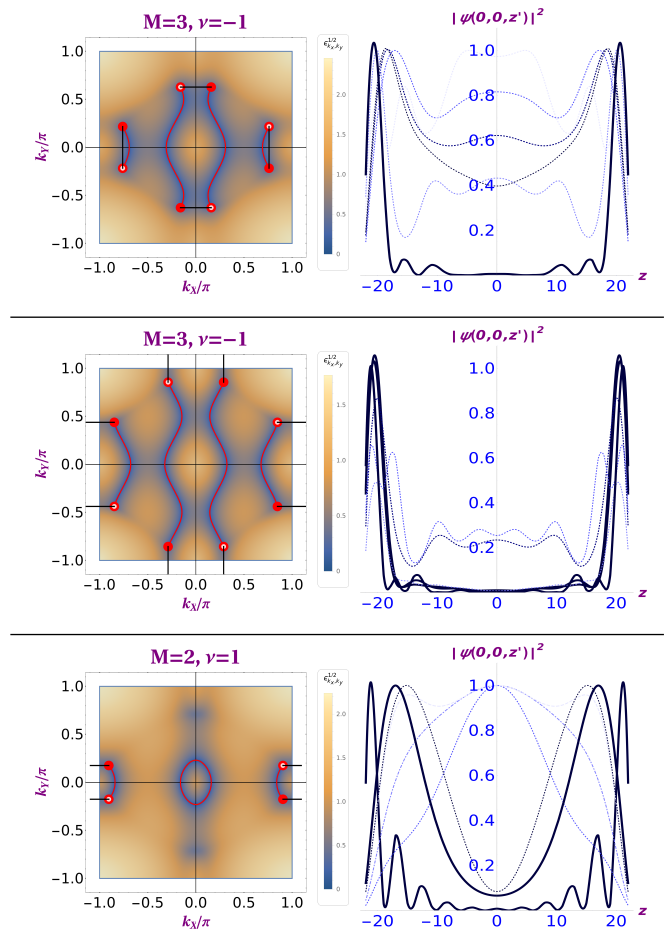


Figure 3. Left column: Color plots of the lowest band for a 45-layer slab in the normal state for the points  $\mathbf{t}$ ,  $\mathbf{m}$  and  $\mathbf{b}$  in Fig. 2 defined by  $l = 0.942$ ,  $m_0 = 6.28$  (top),  $l = 0.972$ ,  $m_0 = 5.48$  (middle) and  $l = 0.552$ ,  $m_0 = 6.18$  (bottom). Red filled (empty) circles denote surface projections of right-(left)-handed WNs. Surface projections of geodesics (black lines) connecting anti-chiral WNs at  $k_z = 0$  form  $M$  closed loops along with the FAs (red curves). Right column: Probability densities of six lowest energy states along a  $z$ -oriented vortex in a  $31 \times 31 \times 45$ -site system. Bold and dotted lines mark states with energies  $E < 5.0 \times 10^{-3}$ , considered "zero energy", and  $E > 1.0 \times 10^{-2}$ .

- [1] Jason Alicea. New directions in the pursuit of majorana fermions in solid state systems. *Reports on Progress in Physics*, 75(7), 2012. ISSN 00344885. doi:10.1088/0034-4885/75/7/076501. URL <https://iopscience.iop.org/article/10.1088/0034-4885/75/7/076501>. (document)
- [2] Andreas Aste. A direct road to majorana fields. *Symmetry*, 2(4):1776–1809, 2010. ISSN 20738994. doi:10.3390/sym2041776.
- [3] C.W.J. Beenakker. Search for majorana fermions in super-

- conductors. *Annual Review of Condensed Matter Physics*, 4 (1):113–136, 2013. ISSN 1947-5454. doi:10.1146/annurev-conmatphys-030212-184337. (document)
- [4] Steven R. Elliott and Marcel Franz. Colloquium: Majorana fermions in nuclear, particle, and solid-state physics. *Reviews of Modern Physics*, 87(1), 2015. ISSN 15390756. doi:10.1103/RevModPhys.87.137.
- [2] Liang Fu and C. L. Kane. Superconducting proximity effect and majorana fermions at the surface of a topological insulator. *Physical Review Letters*, 100(9):96407, 2008. ISSN 00319007. doi:10.1103/PhysRevLett.100.096407. (document), B 2
- [3] Pavan Hosur, Pouyan Ghaemi, Roger S. K. Mong, and Ashvin Vishwanath. Majorana modes at the



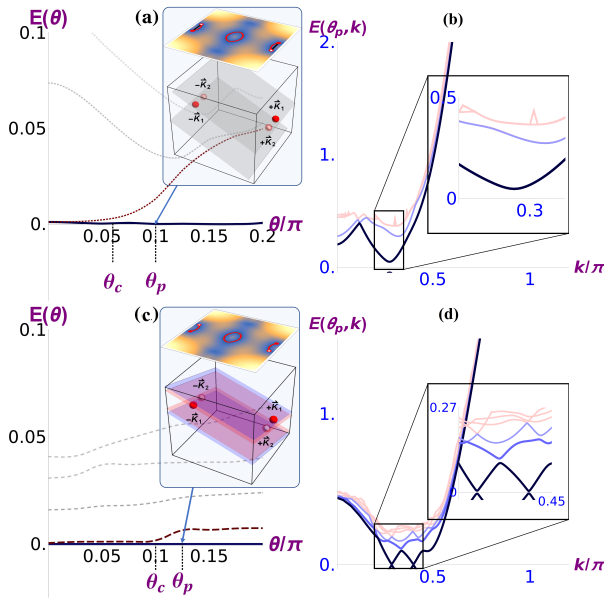


Figure 4. Topological phase transitions upon tilting the  $M = 2$  trivial vortex in Fig. 3 (bottom) obtained by diagonalization in real-space (a, c) and  $k$ -space (b, d). (a) Tilting about the  $x$ -axis produces  $M = 3$  (inset) and gaps out one of the two MFs at  $\theta_c \approx 0.06\pi$ . (b) At  $\theta_p = 0.1\pi$ , the bulk vortex is gapped, so the surviving MF in (a) at  $\theta > \theta_c$  is protected and the vortex is topological. (c, d) Analogous figures for tilting about  $x + y = z = 0$ . In (c), a small gap opens for one MF at  $\theta_c \approx 0.1\pi$  while the surface has open Fermi-geodesic arcs (inset). (d) The bulk vortex is gapless, indicating that the gap in (c) is a finite size gap.

ends of superconductor vortices in doped topological insulators. *Physics Review Letters*, 107:097001, Aug 2011. doi:10.1103/PhysRevLett.107.097001. URL <https://link.aps.org/doi/10.1103/PhysRevLett.107.097001>. (document)

- [5] A Yu Kitaev. Unpaired majorana fermions in quantum wires. *Physics-Uspeski*, 44(10S):131–136, Oct 2001. doi:10.1070/1063-7869/44/10s/s29. URL <https://doi.org/10.10702F1063-78692F442F10s2Fs29>. (document), C
- [8] Martin Leijnse and Karsten Flensberg. Introduction to topological superconductivity and majorana fermions. *Semiconductor Science and Technology*, 27(12), 2012. ISSN 02681242. doi:10.1088/0268-1242/27/12/124003. (document)
- [9] Qin Liu, Chen Chen, Tong Zhang, Rui Peng, Ya Jun Yan, Chen Hao Ping Wen, Xia Lou, Yu Long Huang, Jin Peng Tian, Xiao Li Dong, Guang Wei Wang, Wei Cheng Bao, Qiang Hua Wang, Zhi Ping Yin, Zhong Xian Zhao, and Dong Lai Feng. Robust and clean majorana zero mode in the vortex core of high-temperature superconductor (li0.84fe0.16)ohfese. *Physical Review X*, 8(4):41056, 2018. ISSN 21603308. doi:10.1103/PhysRevX.8.041056. URL <https://doi.org/10.1103/PhysRevX.8.041056>.
- [10] Xiao Ping Liu, Yuan Zhou, Yi Fei Wang, and Chang De Gong. Characterizations of topological superconductors: Chern numbers, edge states and majorana zero modes. *New Journal of Physics*, 19(9), 2017. ISSN 13672630. doi:10.1088/1367-2630/aa8022.
- [11] Roman M. Lutchyn, Tudor D. Stanescu, and S. Das Sarma. Search for majorana fermions in multiband semiconducting nanowires. *Physical Review Letters*, 106(12):1–4, 2011. ISSN 00319007. doi:10.1103/PhysRevLett.106.127001. (document)
- [12] Ning Ma. Majorana fermions in condensed matter: An outlook. *Physica B: Condensed Matter*, 512(January):100–101, 2017. ISSN 09214526. doi:10.1016/j.physb.2017.01.028.
- [13] N. Mohanta and A. Taraphder. Topological superconductivity and majorana bound states at the laal03/srtio3 interface. *Epl*, 108(6), 2014. ISSN 12864854. doi:10.1209/0295-5075/108/60001.
- [14] V. Mourik, K. Zuo, S. M. Frolov, S. R. Plissard, E. P.A.M. Bakkers, and L. P. Kouwenhoven. Signatures of majorana fermions in hybrid superconductor-semiconductor nanowire devices. *Science*, 336(6084):1003–1007, 2012. ISSN 10959203. doi:10.1126/science.1222360. (document)
- [15] Stevan Nadj-Perge, Ilya K. Drozdov, Jian Li, Hua Chen, Sangjun Jeon, Jungpil Seo, Allan H. MacDonald, B. Andrei Bernevig, and Ali Yazdani. Observation of majorana fermions in ferromagnetic atomic chains on a superconductor. *Science*, 346(6209):602–607, 2014. ISSN 10959203. doi:10.1126/science.1259327. URL <https://doi.org/10.1126/science.1259327>.
- [16] Xiao Liang Qi and Shou Cheng Zhang. Topological insulators and superconductors. *Reviews of Modern Physics*, 83(4), 2011. ISSN 00346861. doi:10.1103/RevModPhys.83.1057. URL <https://doi.org/10.1103/RevModPhys.83.1057>. (document)
- [4] N. Read and Dmitry Green. Paired states of fermions in two dimensions with breaking of parity and time-reversal symmetries and the fractional quantum hall effect. *Physical Review B - Condensed Matter and Materials Physics*, 2000. ISSN 1550235X. doi:10.1103/PhysRevB.61.10267. URL <https://doi.org/10.1103/PhysRevB.61.10267>. B 2
- [18] Leonid P. Rokhinson, Xinyu Liu, and Jacek K. Furdyna. The fractional a.c. josephson effect in a semiconductor-superconductor nanowire as a signature of majorana particles. *Nature Physics*, 8(11):795–799, 2012. ISSN 17452481. doi:10.1038/nphys2429. URL <http://dx.doi.org/10.1038/nphys2429>. (document)
- [19] Masatoshi Sato and Satoshi Fujimoto. Existence of majorana fermions and topological order in nodal superconductors with spin-orbit interactions in external magnetic fields. *Physical Review Letters*, 105(21):1–4, 2010. ISSN 00319007. doi:10.1103/PhysRevLett.105.217001. URL <https://doi.org/10.1103/PhysRevLett.105.217001>.
- [20] Masatoshi Sato and Yoichi Ando. Topological superconductors: A review. *Reports on Progress in Physics*, 80(7):1–45, 2017. ISSN 00344885. doi:10.1088/1361-6633/aa6ac7. URL <https://doi.org/10.1088/1361-6633/aa6ac7>. (document)
- [21] Tudor D. Stanescu, Jay D. Sau, Roman M. Lutchyn, and S. Das Sarma. Proximity effect at the superconductor-topological insulator interface. *Physical Review B - Condensed Matter and Materials Physics*, 2010. ISSN 10980121. doi:10.1103/PhysRevB.81.241310. (document)
- [22] Gang Xu, Biao Lian, Peizhe Tang, Xiao-Liang

- Qi, and Shou-Cheng Zhang. Topological superconductivity on the surface of fe-based superconductors. *Physical Review Letters*, 117:047001, Jul 2016. doi:10.1103/PhysRevLett.117.047001. URL <https://link.aps.org/doi/10.1103/PhysRevLett.117.047001>. (document)
- [23] T. Machida, Y. Sun, S. Pyon, S. Takeda, Y. Kohsaka, T. Hanaguri, T. Sasagawa, and T. Tamegai. Zero-energy vortex bound state in the superconducting topological surface state of fe(se,te). *Nature Materials*, 18(8):811–815, 2019. doi:10.1038/s41563-019-0397-1. URL <https://doi.org/10.1038/s41563-019-0397-1>.
- [24] Lingyuan Kong, Shiyu Zhu, Michal Papaj, Hui Chen, Lu Cao, Hiroki Isobe, Yuqing Xing, Wenyao Liu, Dongfei Wang, Peng Fan, Yujie Sun, Shixuan Du, John Schneeloch, Ruidan Zhong, Genda Gu, Liang Fu, Hong-Jun Gao, and Hong Ding. Half-integer level shift of vortex bound states in an iron-based superconductor. *Nature Physics*, 15(11):1181–1187, 2019. doi:10.1038/s41567-019-0630-5. URL <https://doi.org/10.1038/s41567-019-0630-5>.
- [25] Dongfei Wang, Lingyuan Kong, Peng Fan, Hui Chen, Shiyu Zhu, Wenyao Liu, Lu Cao, Yujie Sun, Shixuan Du, John Schneeloch, Ruidan Zhong, Genda Gu, Liang Fu, Hong Ding, and Hong-Jun Gao. Evidence for majorana bound states in an iron-based superconductor. *Science (New York, N.Y.)*, 2018. ISSN 1095-9203. doi:10.1126/science.aao1797. URL <https://doi.org/10.1126/science.aao1797>. (document)
- [26] Peng Zhang, Peng Zhang, Koichiro Yaji, Takahiro Hashimoto, Yuichi Ota, Takeshi Kondo, Kozo Okazaki, Zhijun Wang, Jinsheng Wen, G. D. Gu, Hong Ding, Shik Shin, Peng Zhang, Koichiro Yaji, Takahiro Hashimoto, Yuichi Ota, Takeshi Kondo, Kozo Okazaki, Zhijun Wang, Jinsheng Wen, G. D. Gu, Hong Ding, and Shik Shin. Observation of topological superconductivity on the surface of an iron-based superconductor. *Science*, 360(April):182, 2018. ISSN 10959203. doi:10.1126/science.aan4596. URL <https://doi.org/10.1126/science.aan4596>. (document)
- [27] Conyers Herring. Accidental degeneracy in the energy bands of crystals. *Phys. Rev.*, 52:365–373, Aug 1937. doi:10.1103/PhysRev.52.365. URL <https://link.aps.org/doi/10.1103/PhysRev.52.365>. (document)
- [28] G.E. Volovik. *The Universe in a Helium Droplet*. International Series of Monographs on Physics. OUP Oxford, 2009. ISBN 9780199564842. URL <https://books.google.com/books?id=6uj76kFJOHEC>.
- [29] Xiangang Wan, Ari M. Turner, Ashvin Vishwanath, and Sergey Y. Savrasov. Topological semimetal and fermi-arc surface states in the electronic structure of pyrochlore iridates. *Physical Review B*, 83:205101, May 2011. doi:10.1103/PhysRevB.83.205101. URL <https://link.aps.org/doi/10.1103/PhysRevB.83.205101>.
- [30] N. P. Armitage, E. J. Mele, and Ashvin Vishwanath. Weyl and dirac semimetals in three-dimensional solids. *Reviews of Modern Physics*, 2018. ISSN 15390756. doi:10.1103/RevModPhys.90.015001. URL <https://doi.org/10.1103/RevModPhys.90.015001>. (document)
- [31] P. Hosur and X. Qi. Recent developments in transport phenomena in Weyl semimetals. *Comptes Rendus Physique*, 14(9-10), 2013. ISSN 16310705. doi:10.1016/j.crhy.2013.10.010. URL <https://doi.org/10.1016/j.crhy.2013.10.010>. (document)
- [32] A. A. Burkov. Anomalous hall effect in weyl metals. *Physical Review Letters*, 113:187202, Oct 2014. doi:10.1103/PhysRevLett.113.187202. URL <https://link.aps.org/doi/10.1103/PhysRevLett.113.187202>.
- [33] A A Burkov. Weyl Metals. *Annual Review of Condensed Matter Physics*, 9(1):359–378, 2018. ISSN 1947-5454. doi:10.1146/annurev-conmatphys-033117-054129. URL <https://doi.org/10.1146/annurev-conmatphys-033117-054129>.
- [34] A A Burkov. Chiral anomaly and transport in Weyl metals. *Journal of Physics: Condensed Matter*, 27(11):113201, feb 2015. doi:10.1088/0953-8984/27/11/113201. URL <https://doi.org/10.1088/2F0953-8984/2F27/2F11/2F113201>.
- [35] Y Chen, Si Wu, and A A Burkov. Axion response in Weyl semimetals. *Physical Review B*, 88(12):125105, sep 2013. doi:10.1103/PhysRevB.88.125105. URL <http://link.aps.org/doi/10.1103/PhysRevB.88.125105>.
- [36] A A Zyuzin and A A Burkov. Topological response in Weyl semimetals and the chiral anomaly. *Physical Review B*, 86(11):115133, sep 2012. doi:10.1103/PhysRevB.86.115133. URL <http://link.aps.org/doi/10.1103/PhysRevB.86.115133>.
- [37] P. Hosur and X.-L. Qi. Tunable circular dichroism due to the chiral anomaly in Weyl semimetals. *Physical Review B - Condensed Matter and Materials Physics*, 91(8), 2015. ISSN 1550235X. doi:10.1103/PhysRevB.91.081106. URL <https://doi.org/10.1103/PhysRevB.91.081106>.
- [38] Jin Hu, Su-Yang Xu, Ni Ni, and Zhiqiang Mao. Transport of Topological Semimetals. *Annual Review of Materials Research*, 49(1):207–252, 2019. doi:10.1146/annurev-matsci-070218-010023. URL <https://doi.org/10.1146/annurev-matsci-070218-010023>.
- [39] Fernando de Juan, Adolfo G Grushin, Takahiro Morimoto, and Joel E Moore. Quantized circular photogalvanic effect in Weyl semimetals. *Nature Communications*, 8(1):15995, 2017. doi:10.1038/ncomms15995. URL <https://doi.org/10.1038/ncomms15995>.
- [40] Takuro Kobayashi, Taiki Matsushita, Takeshi Mizushima, Atsushi Tsuruta, and Satoshi Fujimoto. Negative Thermal Magnetoresistivity as a Signature of a Chiral Anomaly in Weyl Superconductors. *Physical Review Letters*, 121(20):207002, 2018. ISSN 10797114. doi:10.1103/PhysRevLett.121.207002. URL <https://doi.org/10.1103/PhysRevLett.121.207002>.
- [41] Karl Landsteiner. Anomalous transport of Weyl fermions in Weyl semimetals. *Physical Review B*, 89(7):75124, feb 2014. doi:10.1103/PhysRevB.89.075124. URL <http://link.aps.org/doi/10.1103/PhysRevB.89.075124>.
- [42] Hailong Li, Haiwen Liu, Hua Jiang, and X C Xie. 3D Quantum Hall Effect Manipulated by Chiral Landau Levels in Weyl Semimetals. *arXiv*, page 2003.00216, 2020.
- [43] R Loganayagam and Piotr Surówka. Anomaly/transport in an Ideal Weyl gas. *Journal of High Energy Physics*, 2012(4):97, apr 2012. ISSN 1029-8479. doi:10.1007/JHEP04(2012)097. URL [https://doi.org/10.1007/JHEP04\(2012\)097](https://doi.org/10.1007/JHEP04(2012)097).
- [44] Naoto Nagaosa, Takahiro Morimoto, and Yoshinori Tokura.

- Transport, magnetic and optical properties of Weyl materials. *Nature Reviews Materials*, 5(8):621–636, 2020. doi:10.1038/s41578-020-0208-y. URL <https://doi.org/10.1038/s41578-020-0208-y>.
- [45] Anna Corinna Niemann, Johannes Gooth, Shu Chun Wu, Svenja Bäbler, Philip Sergeius, Ruben Hühne, Bernd Rellinghaus, Chandra Shekhar, Vicky Süß, Marcus Schmidt, Claudia Felser, Binghai Yan, and Kornelius Nielsch. Chiral magnetoresistance in the Weyl semimetal NbP. *Scientific Reports*, 7(November 2016):3–8, 2017. ISSN 20452322. doi:10.1038/srep43394. URL <http://dx.doi.org/10.1038/srep43394>. (document)
- [46] Pallab Goswami, Girish Sharma, and Sumanta Tewari. Optical activity as a test for dynamic chiral magnetic effect of Weyl semimetals. *Physical Review B*, 92(16):161110, oct 2015. doi:10.1103/PhysRevB.92.161110. URL <https://link.aps.org/doi/10.1103/PhysRevB.92.161110>.
- [47] Chao-Xing Liu, Peng Ye, and Xiao-Liang Qi. Chiral gauge field and axial anomaly in a Weyl semimetal. *Physical Review B*, 87(23):235306, jun 2013. doi:10.1103/PhysRevB.87.235306. URL <http://link.aps.org/doi/10.1103/PhysRevB.87.235306>.
- [48] K.-Y. Yang, Y.-M. Lu, and Y Ran. Quantum Hall effects in a Weyl semimetal: Possible application in pyrochlore iridates. *Physical Review B*, 84(7):75129, aug 2011. doi:10.1103/PhysRevB.84.075129. URL <https://doi.org/10.1103/PhysRevB.84.075129>.
- [49] Chandra Shekhar, Ajaya K Nayak, Yan Sun, Marcus Schmidt, Michael Nicklas, Inge Leermakers, Uli Zeitler, Yurii Skourski, Jochen Wosnitza, Zhongkai Liu, Yulin Chen, Walter Schnelle, Horst Borrmann, Yuri Grin, Claudia Felser, and Binghai Yan. Extremely large magnetoresistance and ultrahigh mobility in the topological Weyl semimetal candidate NbP. *Nature Physics*, 11(8):645–649, 2015. doi:10.1038/nphys3372. URL <https://doi.org/10.1038/nphys3372>.
- [50] Kabyashree Sonowal, Ashutosh Singh, and Amit Agarwal. Giant optical activity and kerr effect in type-i and type-ii weyl semimetals. *Phys. Rev. B*, 100:085436, Aug 2019. doi:10.1103/PhysRevB.100.085436. URL <https://link.aps.org/doi/10.1103/PhysRevB.100.085436>.
- [51] D T Son and B Z Spivak. Chiral anomaly and classical negative magnetoresistance of Weyl metals. *Physical Review B*, 88(10):104412, sep 2013. doi:10.1103/PhysRevB.88.104412. URL <http://link.aps.org/doi/10.1103/PhysRevB.88.104412>.
- [52] C J Tabert, J P Carbotte, and E J Nicol. Optical and transport properties in three-dimensional Dirac and Weyl semimetals. *Physical Review B*, 93(8), 2016. ISSN 24699969. doi:10.1103/PhysRevB.93.085426. URL <https://doi.org/10.1103/PhysRevB.93.085426>.
- [53] M M Vazifeh and M Franz. Electromagnetic Response of Weyl Semimetals. *Physical Review Letters*, 111(2):27201, jul 2013. doi:10.1103/PhysRevLett.111.027201. URL <http://link.aps.org/doi/10.1103/PhysRevLett.111.027201>.
- [54] Shuo Wang, Ben Chuan Lin, An Qi Wang, Da Peng Yu, and Zhi Min Liao. Quantum transport in Dirac and Weyl semimetals: a review. *Advances in Physics: X*, 2(3):518–544, 2017. ISSN 23746149. doi:10.1080/23746149.2017.1327329. URL <http://dx.doi.org/10.1080/23746149.2017.1327329>.
- [55] Huichao Wang and Jian Wang. Electron transport in Dirac and Weyl semimetals. *Chinese Physics B*, 27(10):107402, oct 2018. doi:10.1088/1674-1056/27/10/107402. URL <https://doi.org/10.1088/2F1674-1056/2F27/2F10/2F107402>.
- [56] Shou-Cheng Zhang Min Lv. Dielectric Function, Friedel Oscillation and Plasmons in Weyl Semimetals. *International Journal of Modern Physics B*, 27(25):1350177, 2013.
- [57] H B Nielsen and M Ninomiya. The Adler-Bell-Jackiw anomaly and Weyl fermions in a crystal. *Physics Letters B*, 130(6):389–396, 1983. ISSN 0370-2693. doi:10.1016/0370-2693(83)91529-0. URL [https://doi.org/10.1016/0370-2693\(83\)91529-0](https://doi.org/10.1016/0370-2693(83)91529-0). (document)
- [58] Lijun Meng, Jiafang Wu, Jianxin Zhong, and Rudolf A. Romer. A type of robust superlattice type-i weyl semimetal with four weyl nodes. *Nanoscale*, 11:18358–18366, 2019. doi:10.1039/C9NR04551A. URL <http://dx.doi.org/10.1039/C9NR04551A>. (document)
- [59] Hongming Weng, Chen Fang, Zhong Fang, B Andrei Bernevig, and Xi Dai. Weyl Semimetal Phase in Noncentrosymmetric Transition-Metal Monophosphides. *Physical Review X*, 5(1):11029, mar 2015. doi:10.1103/PhysRevX.5.011029. URL <https://link.aps.org/doi/10.1103/PhysRevX.5.011029>.
- [60] Jianpeng Liu and David Vanderbilt. Weyl semimetals from noncentrosymmetric topological insulators. 155316 (September):1–10, 2014. doi:10.1103/PhysRevB.90.155316. (document)
- [61] Shinsei Ryu, Andreas P. Schnyder, Akira Furusaki, and Andreas W.W. Ludwig. Topological insulators and superconductors: Tenfold way and dimensional hierarchy. *New Journal of Physics*, 12, 2010. ISSN 13672630. doi:10.1088/1367-2630/12/6/065010. URL <https://doi.org/10.1088/1367-2630/12/6/065010>. (document)
- [62] Andreas P. Schnyder, Shinsei Ryu, Akira Furusaki, and Andreas W.W. Ludwig. Classification of topological insulators and superconductors. *AIP Conference Proceedings*, 1134:10–21, 2009. ISSN 0094243X. doi:10.1063/1.3149481. URL <https://doi.org/10.1063/1.3149481>. (document)
- [63] Elio J. König and Piers Coleman. Crystalline-symmetry-protected helical majorana modes in the iron pnictides. *Physical Review Letters*, 122(20), 2019. ISSN 10797114. doi:10.1103/PhysRevLett.122.207001. (document)
- [64] Shengshan Qin, Lunhui Hu, Congcong Le, Jinfeng Zeng, Fu-chun Zhang, Chen Fang, and Jiangping Hu. Quasi-1d topological nodal vortex line phase in doped superconducting 3d dirac semimetals. *Physical Review Letters*, 123:027003, Jul 2019. doi:10.1103/PhysRevLett.123.027003. URL <https://link.aps.org/doi/10.1103/PhysRevLett.123.027003>. (document)
- [65] Zhongbo Yan, Zhigang Wu, and Wen Huang. Vortex end majorana zero modes in superconducting dirac and weyl semimetals. *Phys. Rev. Lett.*, 124:257001, Jun 2020. doi:10.1103/PhysRevLett.124.257001. URL <https://link.aps.org/doi/10.1103/PhysRevLett.124.257001>. (document)
- [66] A. A. Burkov and Leon Balents. Weyl semimetal



- in a topological insulator multilayer. *Physical Review Letters*, 107(12):1–4, 2011. ISSN 00319007. doi: 10.1103/PhysRevLett.107.127205. ([document](#))
- [67] See supplementary material at <http://link.aps.org/supplemental> for further details on calculation. ([document](#))
- [68] Peng Zhang, Zhijun Wang, Xianxin Wu, Koichiro Yaji, Yukiaki Ishida, Yoshimitsu Kohama, Guangyang Dai, Yue Sun, Cedric Bareille, Kenta Kuroda, Takeshi Kondo, Kozo Okazaki, Koichi Kindo, Xiancheng Wang, Changqing Jin, Jiangping Hu, Ronny Thomale, Kazuki Sumida, Shilong Wu, Koji Miyamoto, Taichi Okuda, Hong Ding, G. D. Gu, Tsuyoshi Tamegai, Takuto Kawakami, Masatoshi Sato, and Shik Shin. Multiple topological states in iron-based superconductors. *Nature Physics*, 15(1):41–47, 2019. doi: 10.1038/s41567-018-0280-z. URL <https://doi.org/10.1038/s41567-018-0280-z>. ([document](#))
- [69] Y. M. Dai, H. Miao, L. Y. Xing, X. C. Wang, P. S. Wang, H. Xiao, T. Qian, P. Richard, X. G. Qiu, W. Yu, C. Q. Jin, Z. Wang, P. D. Johnson, C. C. Homes, and H. Ding. Spin-fluctuation-induced non-fermi-liquid behavior with suppressed superconductivity in  $\text{LiFe}_{1-x}\text{Co}_x\text{As}$ . *Phys. Rev. X*, 5:031035, Sep 2015. doi:10.1103/PhysRevX.5.031035. URL <https://link.aps.org/doi/10.1103/PhysRevX.5.031035>. ([document](#))

## Appendix A: Orthorhombic lattice model of a T-WSM

In this section, we analyze the orthorhombic lattice model studied in the main text and describe how to determine its topological nature in the normal state. To recapitulate, the Bloch Hamiltonian is

$$H(\mathbf{k}) = \tau_x \boldsymbol{\sigma} \cdot \mathbf{d}(\mathbf{k}) + \tau_z m(\mathbf{k}) - \tau_y \sigma_z \ell - \mu \quad (\text{A1})$$

where  $d_i = v_i \sin k_i$ ,  $i = x, y, z$ ,  $m(\mathbf{k}) = m_0 - \sum_i \beta_i \cos k_i$  and  $\tau_i$  and  $\sigma_i$  are Pauli matrices acting on orbital and spin space, respectively.  $H(\mathbf{k})$  preserves time-reversal ( $\mathcal{T} = i\sigma_y \mathbb{K}$ ), reflection about the  $xz$  and  $yz$  planes ( $M_{i \rightarrow -i} = \tau_z \sigma_i$ ,  $i = x, y, z$ ) and twofold rotation about the  $z$ -axis ( $R_z = \sigma_z$ ), but breaks inversion ( $\mathcal{I} = \tau_z$ ), reflection about the  $xy$  plane, and twofold rotation about the  $x$  and the  $y$  axes are broken. Its spectrum is given by

$$(E(\mathbf{k}) + \mu)^2 = v_z^2 \sin^2 k_z^2 + m^2(\mathbf{k}) + \left( \sqrt{v_x^2 \sin^2 k_x^2 + v_y^2 \sin^2 k_y^2} \pm \ell \right)^2 \quad (\text{A2})$$

Defining  $X = \cos k_x$ ,  $Y = \cos k_y$ , a quadruplet of Weyl nodes (WNs) appears in the  $k_z = 0$  or  $\pi$  plane at  $(K_x, K_y) = (\pm \cos^{-1} X, \pm \cos^{-1} Y)$  for each intersection between the following ellipse and lines within the unit square  $X \in [-1, 1]$ ,  $Y \in [-1, 1]$

$$v_x^2 X^2 + v_y^2 Y^2 = v_x^2 + v_y^2 - \ell^2 \quad (\text{A3})$$

$$\beta_x X + \beta_y Y = M_{k_z} = m_0 - \beta_z \cos k_z \quad (\text{A4})$$

When the ellipse and line do not intersect within the unit square, the system is an  $\mathcal{T}$ -symmetric insulator. These behaviors are depicted in the top panel of Fig. 5

At  $\ell = 0$ ,  $\mathcal{I}$  is restored, the system is necessarily insulating since the ellipse circumscribes the unit square and the topological nature of the insulator can be deduced from the parity criterion which only depends on  $\text{sgn}[m(\mathbf{k})]$  at the eight time-reversal invariant momenta  $(0/\pi, 0/\pi, 0/\pi)$ . For larger  $\ell$ , the strong topological index of an insulating state can be obtained easily by observing the connectivity of the Fermi arcs on an  $xy$ -surface, as shown in the bottom panel of Fig. 5. Imagine tuning a parameter that creates and subsequently annihilates a quadruplet of WNs. Now, nodes are always created as well as annihilated in pairs of opposite chirality. Moreover, creating a pair of nodes and moving them apart leaves behind a surface Fermi arc that connects the surface projections of the nodes. If the nodes switch partners between creation and annihilation – in other words, if a given right-handed WN is created along with a left-handed WN but annihilates a different left-handed WN – a non-degenerate,  $\mathcal{T}$ -invariant Fermi surface is left behind on the surface. Such a Fermi surface can be viewed as the surface state of a topological insulator doped away from charge neutrality. Therefore, each time WNs switch partners between creation and annihilation, the strong topological index of the bulk insulator toggles.

In the main paper, we choose parameters such that the line defined by  $m(k_z = \pi) = 0$  never intersects the ellipse. Then, all the normal state phase transitions occur via crossings in the  $k_z = 0$  plane, which gives access to trivial and topological insulators as well as T-WSMs with  $N = 1, 2$ .

## Appendix B: Vortex topological invariant in a minimal lattice model

In this section, we use a perturbative scheme to explicitly determine the topological state of the vortex in the lattice model (A1) in the range of parameters which gives  $N = 1$  quadruplet of WNs.

### 1. Reduction to a canonical Weyl Hamiltonian

We begin with the Bloch Hamiltonian (A1) and assume the parameters are chosen so that there is a single quadruplet of WNs, at  $(\pm K_x, \pm K_y, 0)$ . The Bloch Hamiltonian at these points has a higher symmetry, namely,  $[H(\mathbf{K}), \tau_y \sigma_z] = 0$ , so it is convenient to work in the eigenbasis of  $\tau_y \sigma_z$ . For convenience, let us perform a rotation

$$H'(\mathbf{K}) = e^{i\tau_x \pi/4} H(\mathbf{K}) e^{-i\tau_x \pi/4} = \tau_x \boldsymbol{\sigma} \cdot \mathbf{d}(\mathbf{k}) + \tau_z \sigma_z \ell - \mu \quad (\text{B1})$$

which explicitly diagonalizes the term proportional to  $\ell$ . Since  $|\mathbf{d}(\mathbf{K})|^2 = \ell^2$  at the nodes according to Equation (4) of the main paper, the four states at each WN have energies  $2\ell, 0, 0, -2\ell$ . The two zero energy states explicitly are

$$|A'\rangle = \frac{1}{\sqrt{2}} (1, 0, 0, -e^{i\theta_d})^T, \quad |B'\rangle = \frac{1}{\sqrt{2}} (0, e^{i\theta_d}, 1, 0)^T \quad (\text{B2})$$

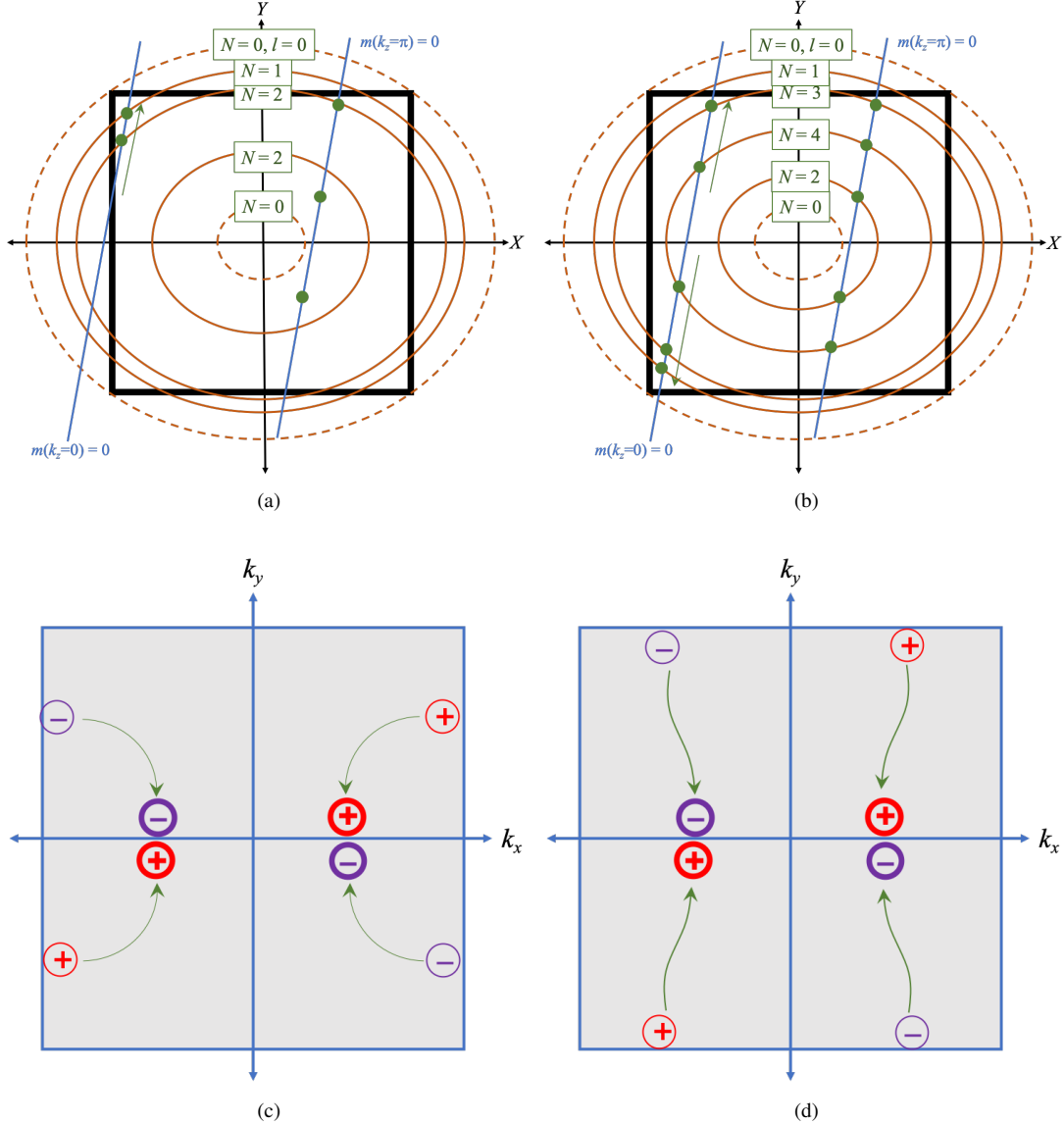


Figure 5. Prescription to determine the number of WN quadruplets ( $N$ ), the Fermi arc structure on the surface and the  $\mathbb{Z}_2$  invariant in the insulating phase in the lattice model (A1). Top:  $X = \cos k_z$ ,  $Y = \cos k_y$  and the ellipses and lines are given by (A3) and (A4), respectively, with smaller  $|\ell|$  defining larger ellipses. Each ellipse-line intersection within the defines a quadruplet of WNs in the plane defining the line. Green arrows indicate the path of the intersections as the ellipse is enlarged. Solid (dashed) ellipses denote T-WSMs with  $N$  quadruplets (insulators with  $N = 0$ ). The  $\ell = 0$  ellipse circumscribes the square and defines an  $\mathcal{I}$ -preserving insulator with  $\mathbb{Z}_2$  indices given by the parity criterion [1]. It has the opposite (same) strong index as the innermost ellipse if exactly one line (no or both lines) intersects a vertical and a horizontal edge of the unit square, as shown on the left (right). Bottom: Brillouin zone of the (001) surface and the effect of moving WNs along the paths indicated in the top panel on the Fermi arcs. For simplicity, only the effect of WNs in the  $k_z = 0$  plane is shown; the effects of  $k_z = \pi$  WNs are identical. Circles with  $\pm$  denote the surface projections of right/left-handed WNs, and their trajectories as the ellipse in the top panel is enlarged are indicated by green arrows. These trajectories trace out the Fermi arcs. If a quadruplet is created at a  $k_x = -k_x$  plane and annihilated on a  $k_y = -k_y$  plane or vice-versa, the Fermi arcs close into a single Fermi surface, implying a change of the bulk strong  $\mathbb{Z}_2$  topological index. If a quadruplet is created and destroyed on a  $k_x = -k_x$  (or  $k_y = -k_y$ ) plane, the  $\mathbb{Z}_2$  invariants corresponding to the ellipse shrunk to a point and the ellipse circumscribing the unit square are the same.



where  $\theta_d = \arg(d_x + id_y)$  and the primes serve as reminders that we have performed a  $e^{i\tau_x\pi/4}$  rotation. The low energy Hamiltonian near the WN in the  $(|A'\rangle, |B'\rangle)^T$  basis is given by

$$H'_W(\mathbf{p}) = (\Sigma_x, \Sigma_y, \Sigma_z) \begin{pmatrix} 0 & 0 & v_z \\ \beta_x \sin K_x & \beta_y \sin K_y & 0 \\ -v_x^2 \ell^{-1} \sin K_x \cos K_x & -v_y^2 \ell^{-1} \sin K_y \cos K_y & 0 \end{pmatrix} \begin{pmatrix} p_x \\ p_y \\ p_z \end{pmatrix} - \mu \quad (\text{B3})$$

where  $\Sigma_i$  are Pauli operators in the  $|A'\rangle, |B'\rangle$  basis. Note that reversing  $K_J$  to get to a different WN is equivalent to reversing  $p_J$  in  $H'_W$ . At  $p_z = 0$ ,  $H'_W$  contains only  $\Sigma_z$  and  $\Sigma_y$ . For convenience, we rotate  $\Sigma_z \rightarrow -\Sigma_x, \Sigma_x \rightarrow \Sigma_z$  to define  $H''_W = e^{i\Sigma_y\pi/4} H'_W e^{-i\Sigma_y\pi/4}$ .  $H''_W$  in the  $p_z = 0$  plane is

$$H''_W(p_z = 0) = \ell^{-1} (\Sigma_x, \Sigma_y) \hat{M} \begin{pmatrix} p_x \\ p_y \end{pmatrix} - \mu \quad (\text{B4})$$

where  $\hat{M} = \begin{pmatrix} v_x^2 \ell^{-1} \sin K_x \cos K_x & v_y^2 \ell^{-1} \sin K_y \cos K_y \\ \beta_x \sin K_x & \beta_y \sin K_y \end{pmatrix}$ . To bring this into a canonical form, we perform a singular value decomposition of  $\hat{M}$

$$\hat{M} = R(\phi_\Sigma) \begin{pmatrix} v_X & 0 \\ 0 & v_Y \end{pmatrix} R^T(\phi_p) \quad (\text{B5})$$

where  $R(\phi) = \begin{pmatrix} \cos \phi & -\sin \phi \\ \sin \phi & \cos \phi \end{pmatrix}$  and  $v_{X,Y} > 0$ . We have assumed that the WNs at  $\pm(K_x, K_y)$  can be brought into a canonical form by proper rotations. This automatically means that the nodes at  $\pm(K_x, -K_y)$  need improper rotations. The necessity of singular value decomposition indicates that the principal axes for  $\mathbf{p}$  and  $\Sigma$  are different, and both differ from the Cartesian axes of the original problem. Moreover,  $v_X \neq v_Y$ , implying that the WN is anisotropic. Nonetheless, this can be brought into a canonical form  $H''_W = v_X \Sigma_X P_X + v_Y \Sigma_Y P_Y - \mu$  through the rotations

$$\begin{pmatrix} P_X \\ P_Y \end{pmatrix} = R^T(\phi_p) \begin{pmatrix} p_x \\ p_y \end{pmatrix} \quad (\text{B6})$$

$$\begin{pmatrix} X \\ Y \end{pmatrix} = R^T(\phi_p) \begin{pmatrix} x \\ y \end{pmatrix} \quad (\text{B7})$$

$$\begin{pmatrix} \Sigma_X \\ \Sigma_Y \end{pmatrix} = R^T(\phi_\Sigma) \begin{pmatrix} \Sigma_x \\ \Sigma_y \end{pmatrix} = e^{-i\Sigma_z\phi_\Sigma/2} \begin{pmatrix} \Sigma_x \\ \Sigma_y \end{pmatrix} e^{i\Sigma_z\phi_\Sigma/2} \quad (\text{B8})$$

## 2. Vortex modes of anisotropic vortex

In the presence of  $s$ -wave superconductivity, the Bogoliubov-deGennes Hamiltonian is given by

$$H''_{BdG}(\mathbf{P}) = \begin{pmatrix} H''_W(\mathbf{P}) & \Delta(\mathbf{R}) \\ \Delta^*(\mathbf{R}) & -H''_W(\mathbf{P}) \end{pmatrix} \quad (\text{B9})$$

in the basis  $\frac{1}{\sqrt{2}} (c_{A'} + c_{B'}, -c_{A'} + c_{B'}, -c_{A'}^\dagger + c_{B'}^\dagger, -c_{A'}^\dagger - c_{B'}^\dagger)^T$ . Furthermore, if the superconductivity develops a vortex  $\Delta(\mathbf{r}) = \Delta_0(r)e^{i\theta}$ , where  $\theta = \arg(x + iy)$ , the pairing term in  $H''_{BdG}$  becomes  $\Delta(\mathbf{R}) = e^{i(\phi_\Sigma + \Theta)} \Delta_0(R)$ , where  $\Theta = \arg(X + iY)$ . If  $v_X = v_Y$ , the problem has a rotational symmetry which can be used to obtain the eigenmodes of  $H''_{BdG}$  analytically. This result is well-known [2–4]. When  $v_X \neq v_Y$ , we can still obtain the eigenmodes analytically in the linear approximation  $\Delta_0(R) = \Delta_0 R/\xi$ , where  $\xi$  is the superconducting coherence length.

We explicitly write

$$H''_{BdG}(\mathbf{P}) = \Pi_z H''_W(\mathbf{P}) + \frac{\Delta_0 R}{\xi} (\Pi_x \cos(\Theta + \phi_\Sigma) - \Pi_y \sin(\Theta + \phi_\Sigma)) \quad (\text{B10})$$

The  $\phi_\Sigma$ -dependence can be eliminated by a  $\Pi_z$ -rotation:

$$H'''_{BdG}(\mathbf{P}) = e^{-i\Pi_z\phi_\Sigma/2} H''_{BdG}(\mathbf{P}) e^{i\Pi_z\phi_\Sigma/2} \quad (\text{B11})$$

$$= \Pi_z H''_W(\mathbf{P}) + \frac{\Delta_0}{\xi} (\Pi_x X - \Pi_y Y) \quad (\text{B12})$$

At  $\mu = 0$ , we can separate the  $X$  and  $Y$  parts of the problem via another rotation. Specifically, define

$$H''''_{BdG}(\mathbf{P}) = e^{i\Pi_y \Sigma_Y \pi/4} H'''_{BdG}(\mathbf{P}) e^{-i\Pi_y \Sigma_Y \pi/4} \quad (\text{B13})$$

$$= \Pi_z \left( v_X \Sigma_X P_X + \frac{\Delta_0}{\xi} \Sigma_Y X \right) - \left( \Pi_x v_Y P_Y + \Pi_y \frac{\Delta_0}{\xi} Y \right) \quad (\text{B14})$$

$$= \sqrt{\frac{2\Delta_0}{\xi}} \begin{pmatrix} & -i\sqrt{v_X} a_X & i\sqrt{v_Y} a_Y & \\ i\sqrt{v_X} a_X^\dagger & & & i\sqrt{v_Y} a_Y \\ -i\sqrt{v_Y} a_Y^\dagger & & & i\sqrt{v_X} a_X \\ & -i\sqrt{v_Y} a_Y^\dagger & -i\sqrt{v_X} a_X^\dagger & \end{pmatrix} \quad (\text{B15})$$

where  $a_J = \sqrt{\frac{\xi}{2\Delta_0 v_J}} \left( \frac{\Delta_0}{\xi} J + i v_J P_J \right)$ ,  $J = X, Y$  is the usual annihilation operator for a quantum harmonic oscillator. The eigenstates of  $H''''_{BdG}$  are of the form  $(|n_X - 1, n_Y - 1\rangle, |n_X, n_Y - 1\rangle, |n_X - 1, n_Y\rangle, |n_X, n_Y\rangle)^T$ . In this basis,

$$H''''_{BdG}(n_X, n_Y) = \sqrt{\frac{2\Delta_0}{\xi}} \begin{pmatrix} & -i\sqrt{v_X n_X} & i\sqrt{v_Y n_Y} & \\ i\sqrt{v_X n_X} & & & i\sqrt{v_Y n_Y} \\ -i\sqrt{v_Y n_Y} & & & i\sqrt{v_X n_X} \\ & -i\sqrt{v_Y n_Y} & -i\sqrt{v_X n_X} & \end{pmatrix} \quad (\text{B16})$$

$$= \sqrt{\frac{2\Delta_0}{\xi}} (\Pi_z \Sigma_Y \sqrt{v_X n_X} + \Pi_x \sqrt{v_Y n_Y}) \quad (\text{B17})$$

Thus, it has the spectrum

$$E(n_X, n_Y) = \pm \sqrt{\frac{2\Delta_0}{\xi} (v_X n_X + v_Y n_Y)} \quad (\text{B18})$$

In particular, the zero mode is given by  $n_X = n_Y = 0$  and has the wavefunction

$$\varphi''''(\mathbf{R}) = (0, 0, 0, |0, 0\rangle)^T \equiv (0, 0, 0, 1)^T f_{00}(X, Y) \quad (\text{B19})$$

where  $f_{00}(X, Y) = \sqrt{\frac{\Delta_0}{\pi \xi \sqrt{v_X v_Y}}} \exp\left[-\frac{\Delta_0}{2\xi} \left(\frac{X^2}{v_X} + \frac{Y^2}{v_Y}\right)\right]$  is the wavefunction for the  $(n_X = 0, n_Y = 0)$  mode of the 2D harmonic oscillator. Undoing the rotations generated by  $\Pi_y \Sigma_Y$ ,  $\Pi_z$ ,  $\Sigma_y$  and the singular value decomposition gives

$$\varphi'(\mathbf{R}) = e^{-i\Sigma_y \pi/4} e^{i\Pi_z \Sigma_z \phi_\Sigma/2} \varphi'' = \frac{1}{\sqrt{2}} e^{-i\Sigma_y \pi/4} (ie^{i\phi_\Sigma}, 0, 0, 1)^T f_{00}(X, Y) \quad (\text{B20})$$

$$\varphi'(x, y) = \frac{1}{2} (ie^{i\phi_\Sigma}, ie^{i\phi_\Sigma}, -1, 1)^T \tilde{f}(x, y) \quad (\text{B21})$$

in the basis  $(c_A, c_B, c_B^\dagger, -c_A^\dagger)$ , where  $\tilde{f}(x, y) = \sqrt{\frac{\Delta_0}{\pi \xi \sqrt{v_X v_Y}}} \exp\left[-\frac{\Delta_0 r^2}{4\xi} \left\{ \left(\frac{1}{v_X} + \frac{1}{v_Y}\right) + \left(\frac{1}{v_X} - \frac{1}{v_Y}\right) \cos[2(\theta + \phi_p)] \right\}\right] \equiv \sqrt{\frac{\Delta_0}{\pi \xi \sqrt{v_X v_Y}}} \exp\left[-\frac{\Delta_0 r^2}{4\xi} \left\{ \frac{1}{v_+} + \frac{1}{v_-} \cos[2(\theta + \phi_p)] \right\}\right]$ .  $\varphi'$  is an eigenstate of charge conjugation:  $\mathbb{C}\varphi' \equiv \Pi_y \Sigma_y \varphi'^* = ie^{-i\phi_\Sigma} \varphi'$  and hence, represents a Majorana mode. In the original basis  $(c_{s\uparrow}, c_{s\downarrow}, c_{p\uparrow}, c_{p\downarrow}, c_{s\downarrow}^\dagger, -c_{s\uparrow}^\dagger, c_{p\downarrow}^\dagger, -c_{p\uparrow}^\dagger)^T$ ,

$$\begin{aligned} \varphi(x, y) &= \frac{e^{-i\pi/4}}{2\sqrt{2}} \left( -e^{i\phi_\Sigma}, ie^{i(\theta_d + \phi_\Sigma)}, -e^{i\phi_\Sigma}, -ie^{i(\theta_d + \phi_\Sigma)}, -ie^{-i\theta_d}, 1, ie^{-i\theta_d}, 1 \right)^T \tilde{f}(x, y) \\ &\equiv \chi \tilde{f}(x, y) \end{aligned} \quad (\text{B22})$$

Finally,  $\chi^\dagger \Pi_z \tau_x \sigma_z \chi = 1$ , so non-zero  $k_z$  induces a dispersion  $E(k_z) = v_z \sin k_z$  and thus produces a CMM.

### 3. Hybridization between CMMs

The Majorana fermions coming from WNs at  $(K_x, -K_y)$ ,  $(-K_x, -K_y)$  and  $(-K_x, K_y)$  can be obtained by applying the symmetry operations  $S_y = i\mathcal{T}M_y = \tau_z \mathbb{K} \otimes y \rightarrow -y$ ,  $S_{xy} = -i\Pi_z M_x M_y = \Pi_z \sigma_z \otimes (x, y) \rightarrow -(x, y)$  and  $S_x = \Pi_z \mathcal{T}M_x = \Pi_z \tau_z \sigma_z \mathbb{K} \otimes x \rightarrow -x$ , respectively. The result after reinstating the fast spatial variation is

$$\psi_{\lambda_x \lambda_y}(x, y) = \frac{1}{2\sqrt{2}} e^{i(\lambda_x K_x x + \lambda_y K_y y - \lambda_x \lambda_y \pi/4)} \sqrt{\frac{\Delta_0}{\pi \xi \sqrt{v_X v_Y}}} \exp \left[ -\frac{\Delta_0 r^2}{4\xi} \left\{ \frac{1}{v_+} + \frac{\cos[2(\theta - \lambda_x \lambda_y \phi_p)]}{v_-} \right\} \right] \times \left( -e^{i\lambda_x \lambda_y \phi_\Sigma}, i\lambda_y e^{i\lambda_x \lambda_y (\theta_d + \phi_\Sigma)}, -\lambda_x \lambda_y e^{i\lambda_x \lambda_y \phi_\Sigma}, -i\lambda_x e^{i\lambda_x \lambda_y (\theta_d + \phi_\Sigma)}, -i\lambda_y e^{-i\lambda_x \lambda_y \theta_d}, 1, i\lambda_x e^{-i\lambda_x \lambda_y \theta_d}, \lambda_x \lambda_y \right)^T$$

where  $\lambda_x = \pm$ ,  $\lambda_y = \pm$ . For  $K_{x,y}\xi \gg 1$ , the leading perturbation from band curvature is given by the matrix elements

$$\begin{aligned} \langle \psi_{\lambda'_x \lambda'_y} | H_2 | \psi_{\lambda_x \lambda_y} \rangle &= e^{i\pi/4(\lambda'_x \lambda'_y - \lambda_x \lambda_y)} \int_{x,y} e^{i[(\lambda_x - \lambda'_x)K_x x + (\lambda_y - \lambda'_y)K_y y]} \varphi_{\lambda'_x \lambda'_y}^\dagger(x, y) \times \\ &\quad \frac{1}{2} \left( p_x^2 \partial_{k_x}^2 H_{BdG}(\lambda_x K_x, \lambda_y K_y) + p_y^2 \partial_{k_y}^2 H_{BdG}(\lambda_x K_x, \lambda_y K_y) \right) \varphi_{\lambda_x \lambda_y}(x, y) \end{aligned} \quad (\text{B23})$$

$$\begin{aligned} &= -\frac{1}{2} e^{i\pi/4(\lambda'_x \lambda'_y - \lambda_x \lambda_y)} \int_{x,y} e^{i[(\lambda_x - \lambda'_x)K_x x + (\lambda_y - \lambda'_y)K_y y]} \varphi_{\lambda'_x \lambda'_y}^\dagger(x, y) \Pi_z \times \\ &\quad \left[ \begin{array}{c} p_x^2 \left( \frac{\lambda_x + \lambda'_x}{2} \tau_x \sigma_x v_x \sin K_x - \tau_z \beta_x \cos K_x \right) + \\ p_y^2 \left( \frac{\lambda_y + \lambda'_y}{2} \tau_x \sigma_y v_y \sin K_y - \tau_z \beta_y \cos K_y \right) \end{array} \right] \varphi_{\lambda_x \lambda_y}(x, y) \end{aligned} \quad (\text{B24})$$

which consists of straightforward Gaussian integrals. First, let us compute the spinor products. In the basis  $(|\chi_{++}\rangle, |\chi_{--}\rangle, |\chi_{-+}\rangle, |\chi_{+-}\rangle)$ , we find

$$(\lambda_i + \lambda_{i'}) \Pi_z \tau_x \sigma_i \rightarrow 0; i = x, y \quad (\text{B25})$$

$$\begin{aligned} \Pi_z \tau_z \rightarrow &\begin{pmatrix} e^{-i\phi_\Sigma} \cos \theta_d \sin(\phi_\Sigma + \theta_d) & -e^{-i\phi_\Sigma} \cos(\phi_\Sigma + \theta_d) \sin \theta_d \\ -e^{-i\phi_\Sigma} \cos(\phi_\Sigma + \theta_d) \sin \theta_d & e^{-i\phi_\Sigma} \cos \theta_d \sin(\phi_\Sigma + \theta_d) \\ 0 & 0 \end{pmatrix} + \\ &\begin{pmatrix} 0 & 0 \\ e^{i\phi_\Sigma} \cos \theta_d \sin(\phi_\Sigma + \theta_d) & -e^{i\phi_\Sigma} \cos(\phi_\Sigma + \theta_d) \sin \theta_d \\ -e^{i\phi_\Sigma} \cos(\phi_\Sigma + \theta_d) \sin \theta_d & e^{i\phi_\Sigma} \cos \theta_d \sin(\phi_\Sigma + \theta_d) \end{pmatrix} \end{aligned} \quad (\text{B26})$$

Note that only CMMs coming from nodes of opposite chiralities mix, in which case  $\lambda'_x \lambda'_y = -\lambda_x \lambda_y$ , and the hybridization is caused by the ‘‘mass’’ term, not the ‘‘kinetic’’ terms, of the Dirac Hamiltonian (A1). Finally, we get the effective Hamiltonian in the basis  $(|\psi_{++}\rangle, |\psi_{--}\rangle, e^{-i\phi_\Sigma} |\psi_{-+}\rangle, e^{-i\phi_\Sigma} |\psi_{+-}\rangle)^T$  as

$$H_{eff} = i \begin{pmatrix} & q_x & q_y \\ & q_y & q_x \\ -q_x & -q_y & \\ -q_y & -q_x & \end{pmatrix} \quad (\text{B27})$$



where  $q_i$  decays as a Gaussian as a function of  $\Delta K_i = K_i - (-K_i)$ . Explicitly,

$$q_x = \frac{(\Delta K_x)^2 \cos \theta_d \sin(\phi_\Sigma + \theta_d)}{2} \exp \left[ -\frac{\xi (\Delta K_x)^2}{2\Delta_0 \left( \frac{1}{v_+} + \frac{\cos 2\phi_p}{v_-} \right)} \right] \times \left( \mathbb{V}_+^2 \left( \frac{1}{v_+} - \frac{\cos 2\phi_p}{v_-} \right)^2 \beta_x \cos K_x + \mathbb{V}_-^2 \frac{\sin^2 2\phi_p}{v_-^2} \beta_y \cos K_y \right) \quad (\text{B28})$$

$$q_y = -\frac{(\Delta K_y)^2 \cos(\phi_\Sigma + \theta_d) \sin \theta_d}{2} \exp \left[ -\frac{\xi (\Delta K_y)^2}{2\Delta_0 \left( \frac{1}{v_+} - \frac{\cos 2\phi_p}{v_-} \right)} \right] \times \left( \mathbb{V}_+^2 \frac{\sin^2 2\phi_p}{v_-^2} \beta_x \cos K_x + \mathbb{V}_-^2 \left( \frac{1}{v_+} + \frac{\cos 2\phi_p}{v_-} \right)^2 \beta_y \cos K_y \right) \quad (\text{B29})$$

to leading order in  $\Delta_0 \xi / (\Delta K_x)^2$  and  $\Delta_0 \xi / (\Delta K_y)^2$ , where  $\mathbb{V}_\pm^2 = (v_X v_Y)^{-1/2} \left( \frac{1}{v_\pm} \pm \frac{\cos 2\phi_p}{v_\mp} \right)^{-1/2} \left( \frac{1}{v_\pm} \mp \frac{\cos 2\phi_p}{v_\mp} \right)^{-5/2}$  has units of velocity-squared. For  $|\Delta K_x| \gg |\Delta K_y|$  and  $|\Delta K_x| \ll |\Delta K_y|$ ,  $Q = \begin{pmatrix} q_x & q_y \\ q_y & q_x \end{pmatrix}$  simplifies to  $\begin{pmatrix} 0 & q_y \\ q_y & 0 \end{pmatrix}$  and  $\begin{pmatrix} q_x & 0 \\ 0 & q_x \end{pmatrix}$ , respectively, so that the vortex topological invariant is

$$\nu = \text{sgn}[\det(Q)] = \begin{cases} -1 & |\Delta K_x| \gg |\Delta K_y| \\ +1 & |\Delta K_x| \ll |\Delta K_y| \end{cases} \quad (\text{B30})$$

Thus, there is vortex phase transition as the WNs “switch partners”, i.e., the nearest WN to a given WN changes.

#### 4. Hybridization gap in the continuum limit

Deep in the topological phase,  $q_x \ll q_y$ , and the eigenvalues of  $H_{eff}$  reduce to  $\pm|q_y|$ . To detect the surface Majorana fermion in this regime, one must thus be at temperatures  $T \ll |q_y|/k_B$ , which we now estimate.

$|q_y|$ , as given by (B29), is straightforward albeit tedious to estimate in the continuum limit  $k_x, k_y \ll 1$ . Restricting to the  $k_z = 0$  plane as done throughout the derivations above, (A3) and (A4), which determine the locations of the WNs, simplify to

$$v_x^2 K_x^2 + v_y^2 K_y^2 = \ell^2 \quad (\text{B31})$$

$$\beta_x K_x^2 + \beta_y K_y^2 = -2m_\Gamma \quad (\text{B32})$$

where  $m_\Gamma = m_0 - \sum_{i=x,y,z} \beta_i$ . Then,  $\hat{M}$ , which defines the non-canonical Weyl Hamiltonian  $H_W''$  in (B4) becomes

$$\hat{M} = \begin{pmatrix} v_x^2 K_x / \ell & v_y^2 K_y / \ell \\ \beta_x K_x & \beta_y K_y \end{pmatrix} = R(\phi_\Sigma) \begin{pmatrix} v_X & 0 \\ 0 & v_Y \end{pmatrix} R^T(\phi_p) \quad (\text{B33})$$

Deep in the topological phase of the vortex where  $K_y^2 \ll K_x^2$ , (B31) implies  $\ell \approx K_x v_x$ . To ensure consistency with (B32), we must fine-tune  $m_\Gamma \approx -\beta_x K_x^2 / 2$ . Note that  $|\ell|, |m_\Gamma| \ll |v_x|, |v_y|$  ensures that the WNs occur in the continuum limit,  $K_{x,y} \ll 1$ . Within the continuum limit,  $K_y \ll K_x$  is enforced by fine-tuning  $\beta_x$  without making any of the individual parameters  $-\ell, v_x, v_y, \beta_x, \beta_y$  and  $m_\Gamma$  further small or large in magnitude. In this regime,  $\hat{M}$  simplifies to

$$\hat{M} \approx \begin{pmatrix} v_x & v_y^2 K_y / v_x K_x \\ \beta_x K_x & \beta_y K_y \end{pmatrix} = R(\phi_\Sigma) \begin{pmatrix} v_X & 0 \\ 0 & v_Y \end{pmatrix} R^T(\phi_p) \quad (\text{B34})$$

where  $v_X, v_Y > 0$ , assuming that the singular value decomposition at  $(K_x, K_y)$  is achieved by proper rotations. Explicitly,

$$v_X \approx \left| v_x^2 + \beta_x^2 K_x^2 + \frac{(v_y^2/K_x + \beta_x \beta_y K_x)^2}{v_x^2 + \beta_x^2 K_x^2} K_y^2 \right|^{1/2} \approx v_x \quad (\text{B35})$$

$$v_Y \approx \frac{|v_y^2 \beta_x / v_x - v_x \beta_y|}{v_x^2 + \beta_x^2 K_x^2} |K_y| \approx \left| \beta_x \frac{v_y^2}{v_x^2} - \beta_y \right| |K_y| \quad (\text{B36})$$

$$|\phi_p| \approx \left| \frac{v_y^2 + \beta_x \beta_y K_x^2}{v_x^2 + \beta_x^2 K_x^2} \frac{K_y}{K_x} \right| \approx \left| \frac{v_y^2 K_y}{v_x^2 K_x} \right| \quad (\text{B37})$$

$$|\phi_\Sigma| \approx \left| \frac{\beta_x^2 K_x^2 + \beta_y^2 K_y^2}{v_x^2 + v_y^4 K_y^2 / v_x^2 K_x^2} \right|^{1/2} \approx \left| \frac{\beta_x K_x}{v_x} \right| \quad (\text{B38})$$

Since  $v_Y/v_X, |\phi_p| \sim O(K_y/K_x) \ll 1$ , this further yields

$$\frac{1}{v_\pm} \approx \pm \frac{1}{v_Y} \quad (\text{B39})$$

$$\mathbb{V}_+ \approx \frac{v_Y}{2\sqrt{2}} \quad (\text{B40})$$

$$\mathbb{V}_- \approx \frac{v_X}{2\sqrt{2}} \quad (\text{B41})$$

$$\frac{\mathbb{V}_+}{\mathbb{V}_-} \approx \frac{v_Y}{v_X} \sim O\left(\frac{K_y}{K_x}\right) \ll 1 \quad (\text{B42})$$

Putting all this together along with  $|\phi_\Sigma| \sim O(K_x) \ll 1$  in the continuum limit and  $|\theta_d| \approx |v_y K_y / v_x K_x| \ll 1$  deep in the topological phase, we get for  $|q_y|$ :

$$|q_y| = \frac{1}{4} \beta_y (\Delta K_y)^2 |\theta_d| \exp \left[ -\frac{\xi v_Y (\Delta K_y)^2}{4\Delta_0} \right] \quad (\text{B43})$$

Assuming typical values for band parameters ( $v_Y \sim v_X/10 \sim 10^4 m/s$ ,  $K_y \sim K_x/10 \sim 0.02 \times 2\pi/a$  with  $a \approx 6.0\text{\AA}$ ,  $v_y = v_x$  so that  $|\theta_d| \sim 0.1$  and  $\beta_y^{-1} \sim$  bare electron mass) and superconducting properties ( $\Delta_0 \sim 5K$  and  $\xi \sim 5nm$ ) gives  $|q_y| \sim 0.1K$  and  $|q_x| \sim 0$  with  $|\Delta K_y \xi| \sim 2 \gtrsim 1$ . The vortex originating from individual WNs is  $\delta \sim \Delta_0 \hbar v_Y / \mu \xi \sim 1K$  for  $\mu \sim 100K$ , so that  $|q_y| \lesssim \delta \lesssim \Delta_0$ , ensuring that we are in the right perturbative regimes. Note that this expression for  $\delta$  differs from the one that follows from (B18); the latter is only valid at  $\mu = 0$  whereas real materials invariably have non-zero  $\mu \gg \Delta_0$  and fall in the regime where the former is valid.

### Appendix C: Level crossings, Pfaffian and Topological phase transitions

In this section, we select representative points on the phase diagram in Fig. 2 of the main paper, explicitly compare the prediction (Equation 1 of the main paper) and the result of calculating the Pfaffian-based invariant [5], and show that topological phase transitions are accompanied by level crossings in the vortex as expected. The results are shown in Fig. 6. All the data points in Fig. 2 of the main paper were obtained using the same Pfaffian-based invariant [5].

- 
- [1] Liang Fu, C L Kane, and E J Mele. Topological Insulators in Three Dimensions. *Physical Review Letters*, 98(10):106803, mar 2007. doi:10.1103/PhysRevLett.98.106803. URL <https://link.aps.org/doi/10.1103/PhysRevLett.98.106803>. 5
  - [2] Liang Fu and C. L. Kane. Superconducting proximity effect and majorana fermions at the surface of a topological insulator. *Physical Review Letters*, 100(9):96407, 2008. ISSN 00319007. doi:10.1103/PhysRevLett.100.096407. (document), B 2
  - [3] Pavan Hosur, Pouyan Ghaemi, Roger S. K. Mong, and Ashvin Vishwanath. Majorana modes at the ends of superconductor vortices in doped topological insulators. *Physics Review Letters*, 107:097001, Aug 2011. doi:10.1103/PhysRevLett.107.097001. URL <https://link.aps.org/doi/10.1103/PhysRevLett.107.097001>. (document)

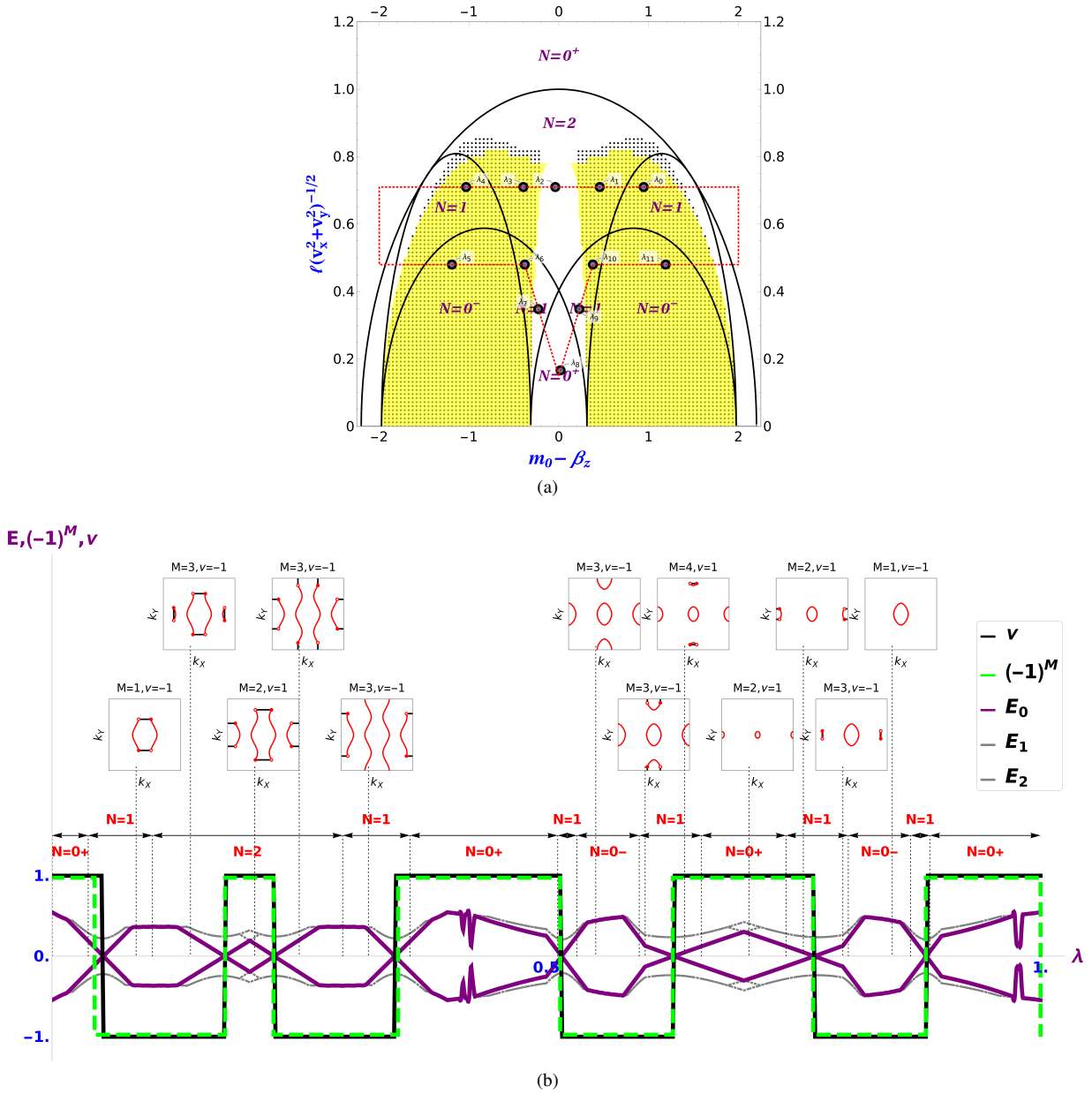


Figure 6. (a) Representative points and the path for which results are presented in (b). (b) Lowest few energies, predicted topological invariant  $(-1)^M$  and the computed invariant  $\nu$  along the path denoted in (a) parameterized by  $\lambda$ . The insets show the FGSs at each representative point. The predicted and computed results show excellent agreement and each phase transition is accompanied by a level crossing at zero energy.

- [4] N. Read and Dmitry Green. Paired states of fermions in two dimensions with breaking of parity and time-reversal symmetries and the fractional quantum hall effect. *Physical Review B - Condensed Matter and Materials Physics*, 2000. ISSN 1550235X. doi:10.1103/PhysRevB.61.10267. URL <https://doi.org/10.1103/PhysRevB.61.10267>. B 2
- [5] A Yu Kitaev. Unpaired majorana fermions in quantum wires. *Physics-Uspekhi*, 44(10S):131–136, Oct 2001. doi:10.1070/1063-7869/44/10s/s29. URL <https://doi.org/10.10702F1063-78692F442F10s2Fs29>. (document), C